Spin-dependent recombination of photoinduced carriers in phthalocyanine/C_{60} heterojunctions

Ichiro Hiromitsu, Yoshiaki Kaimori, Mayuko Kitano, and Takashi Ito
Department of Material Science, Interdisciplinary Faculty of Science and Engineering, Shimane University, Matsue 690-8504, Japan
(Received 28 May 1998)

Spin-dependent recombination of photoinduced carriers in H_2-phthalocyanine (H_2Pc)/C_{60} heterojunctions is studied by electrically detected electron-spin resonance (EDESR) spectroscopy. The EDESR spectrum of the H_2Pc/C_{60} consists of two components *A* and *B*, the *g* values of which are 2.0018 ± 0.0002 and 2.0010 ± 0.0002, respectively. The two components are attributed to exchange-coupled localized electron-hole pairs trapped at different types of recombination centers. Component *A* has spin-flip satellites due to an interaction between the electron (or hole) spin, and its surrounding nuclear spins of protons which belong to the H_2Pc rings. From the satellite intensity, the distance between the electron (or hole) and the protons is estimated to be 4.33 ± 0.25 Å, indicating that the localized pairs for the component *A* locate close to the H_2Pc rings. The spin dynamics of the localized pairs for the component *A* is studied by a microwave recovery experiment, in which the time dependence of the EDESR signal intensity is measured after turning the resonant microwave on and off. A theoretical model of the spin-dependent recombination of the exchange-coupled electron-hole pair is proposed with which the experimental results of the microwave recovery are explained. By a theoretical analysis, it is found that $R\gtrsim1\times10^6$ s^{-1} and $D+W_{sl}=6.2\,(\pm0.8)\times10^4$ s^{-1} for component *A* at room temperature, where *R* is the recombination rate of the localized pair in the $S_z=0$ triplet sublevel, and *D* and W_{sl} are the dissociation and the spin-lattice relaxation rates, respectively, of the pairs in the triplet sublevels. The photocurrent I_2 that is caused by the dissociation of the localized pairs for component *A* is about 5% of the total photocurrent. [S0163-1829(99)02403-0]

I. INTRODUCTION

Electrically detected electron-spin resonance (EDESR), which is also called electrically detected magnetic resonance, is a technique to observe electron-spin resonance (ESR) signal by detecting a change of the photocurrent or conductivity of the sample.[1–4] The change of the photocurrent or conductivity is caused by a change of the recombination probability of the carriers. The recombination probability is spin dependent, so that it is affected by the occurrence of the ESR transition, which alters the spin states. The sensitivity of EDESR is 10^3-10^4 times higher than conventional ESR,[5–7] so that EDESR is a powerful experimental technique to study the recombination mechanism in small-volume systems like thin films or heterojunctions.

In some EDESR experiments, a change of the photocurrent or conductivity by a factor of $\sim10^{-4}$ (Refs. 8 and 9) or even $\sim10^{-1}$ (Ref. 7) is observed as a result of the ESR transition, which is due to an increase of the recombination probability of photoinduced or electrically injected carriers. The changes of 10^{-4} as well as 10^{-1} are quite large, and cannot be explained if the spin states of the carriers obey the simple Boltzmann statistics.[1] Kaplan, Solomon, and Mott showed[2] that such a large change of the photocurrent or conductivity can be explained by a localized electron-hole pair model, in which an electron and a hole make a localized pair for a certain period. Since the pairs in the singlet spin configuration can disappear by recombination, the fraction of the triplet pairs becomes larger than that expected by the Boltzmann distribution. By applying the resonant microwave, a net transition occurs from the triplet state to the singlet so that the recombination is enhanced.

Kaplan, Solomon, and Mott assumed[2] no exchange interaction between the electron and the hole, because, if the exchange interaction is stronger than the difference of the resonance frequencies of the electron and the hole, the ESR transition occurs between the triplet sublevels and does not affect the number of the singlet pairs. If the assumption of Ref. 2 is correct, the electron and hole take part in the ESR transition independently, so that a separate observation of the EDESR signals of the electron and the hole should be possible in principle. In most of the EDESR spectra reported so far, however, only a single line is observed, and the signals of the electron and the hole are not isolated. This suggests that there exists a significant exchange interaction which makes the signals of the electron and the hole meet in one EDESR line.[10] Assuming that the difference between the *g* values of the electron and hole is in the order of 0.001, an exchange interaction of 10^{-3} K is strong enough to make a single EDESR line. Since the electron and hole in a localized pair should be in close proximity so as to take part in the recombination, such an exchange interaction can certainly exist. Thus, the model of Ref. 2 should be generalized to the case when exchange interaction exists. Dyakonov *et al.* suggested[7] that a selective intersystem crossing between the triplet and singlet states may explain the EDESR effect under the exchange interaction, but no quantitative analysis has been presented. Furthermore, when EDESR is measured from the change of the photocurrent, there should be carriers that do not experience localized pairs. The problem of how many percent of the photocurrent is related to the localized pairs has never been considered. Thus, the basic mechanism that gives rise to the EDESR signal has not been completely understood.

In this paper, a comprehensive EDESR study is done for H_2Pc/C_{60} heterojunction. The photovoltaic characteristics of

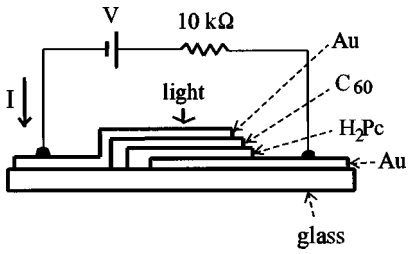

FIG. 1. Scheme of a H_2Pc/C_{60} heterojunction.

the H_2Pc/C_{60} heterojunction have been reported recently:[5] The H_2Pc/C_{60} is a typical donor-acceptor-type[11] photocell, with a conversion efficiency of 0.02%. The photovoltaic effect occurs by a photo-excitation of H_2Pc and/or C_{60} in the interface region, followed by a charge separation in which the electron and the hole diffuse to the C_{60} (acceptor) and the H_2Pc (donor) layers, respectively. A preliminary EDESR study was also done previously[5] in which a decrease of the photocurrent by a factor of $\sim 10^{-4}$ was observed by applying a resonant microwave. In the present study, a more complete EDESR measurement is done with an improved sensitivity. It will be shown that the EDESR spectrum is made by an overlap of two components, one of which has spin-flip satellites by an interaction between an electron (or hole) spin and the nearby nuclear spins of protons. The observation of the spin-flip satellites is quite exceptional, and an analysis of the satellite intensity will give us some information on the location of the detected carrier spins. A measurement of microwave recovery of the EDESR intensity allows us a direct observation of the spin dynamics of the localized pairs. A theoretical model of the spin-dependent recombination is proposed for the case of finite exchange interaction between the electron and the hole, which explains the experimental results of the microwave recovery. A clear insight on the mechanism of the spin-dependent recombination in the H_2Pc/C_{60} heterojunction will be obtained.

II. EXPERIMENT

H_2Pc was purchased from Nacalai Tesque Inc. and was used after subliming twice in vacuum. C_{60} (99.95%) was purchased from MER Corp., and was used without further purification.

The arrangement of the thin films in the heterojunction system is shown in Fig. 1. A gold film of 25-nm thickness was evaporated on a glass substrate of $1\times18\times0.15$ mm^3 under a pressure below 1×10^{-4} Pa, followed by the H_2Pc and the C_{60} films each of 120-nm thickness. On top of the C_{60} film, another gold electrode was evaporated of about 25-nm thickness. The rates of the deposition were 0.02, 0.3, and 0.15 nm/sec for the Au, H_2Pc, and C_{60} films, respectively, monitored by a quartz oscillator (ULVAC CRTM5000). The active area for the photovoltaic effect is about 2 mm^2. In the present study, the glass substrate was mainly used instead of the quartz substrate, the latter having been used in the previous study.[5] No difference is seen in the EDESR spectrum as well as the photovoltaic characteristics between the two cases of the glass and the quartz substrates. In the measurements, the sample was kept in vacuum in a quartz tube.

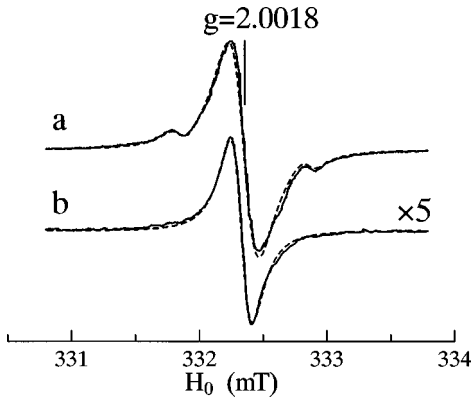

FIG. 2. *X*-band (9.3 GHz) EDESR spectra of a H_2Pc/C_{60} heterojunction at room temperature. The microwave power incident to the cavity is 25 mW for *a* and 0.38 mW for *b*. The broken line for *a* is a simulated one assuming Lorentzian line shapes for the central and the satellite lines. The broken line for *b* is a simulated one with a Lorentzian line shape.

The EDESR measurement was done on home built *X* band (9.3 GHz) and *K*-band (23 GHz) spectrometers using a 600-Hz field modulation of 0.05 mT. The voltage across the 10-kΩ load in Fig. 1 was fed to a lock-in amplifier which was synchronous to the 600-Hz field modulation. The bias voltage was $V=0$ unless otherwise noted. A TE_{101} rectangular cavity and a TE_{011} cylindrical cavity were used for the *X*- and *K*-band measurements, respectively, which had grids for the illumination of the sample. The illumination was done with a 500-W Xe lamp from the C_{60} side, as shown in Fig. 1. The light in the IR region of $\lambda>900$ nm was cut off using a glass filter (Toshiba IRA-25S). The maximum microwave power incident to the cavity was 25 mW for both the *X*- and *K*-band measurements.

For the microwave recovery measurement of the photocurrent, a 25-mW microwave in the *X*-band region was turned on and off using a *p-i-n* diode whose switching time was 0.1 μs. The voltage across the 10-kΩ load of the sample was fed to a differential preamplifier, the output of which was monitored on a digital oscilloscope. The obtained transient signal was accumulated on a personal computer. Typically 10 000-times accumulation was needed in order to obtain a sufficient signal-to-noise ratio. For the baseline correction, the recovery curve with the magnetic field out of the resonance was subtracted from that at the center of the resonance.

III. RESULTS

A. EDESR

Figure 2 shows the *X*-band (9.3 GHz) EDESR spectra of the H_2Pc/C_{60} heterojunction at room temperature, with microwave powers of 25 and 0.38 mW. The spectrum with 25 mW has a 30% broader peak-to-peak linewidth than that with 0.38 mW, which is due to the microwave-power saturation. Two satellites are seen in the 25-mW spectrum. A least-squares fitting was done for the 25-mW spectrum, assuming that the central line and the two satellites have Lorentzian line shapes, the result of which is shown in Fig. 2. The spacing between the satellite and the central line is

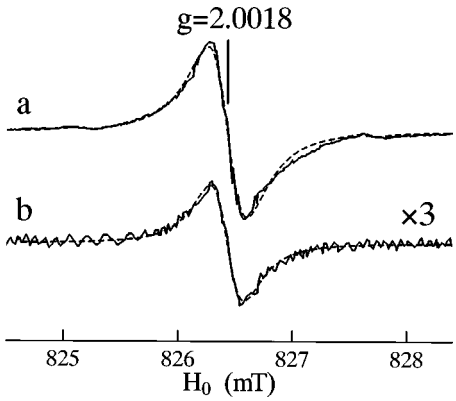

FIG. 3. *K*-band (23 GHz) EDESR spectra of a H_2Pc/C_{60} heterojunction at room temperature. The microwave power incident to the cavity is 25 mW for *a* and 0.78 mW for *b*. The broken line for *a* is a simulated one assuming Lorentzian line shapes for the central and the satellite lines. The broken line for *b* is a simulated one with a Lorentzian line shape.

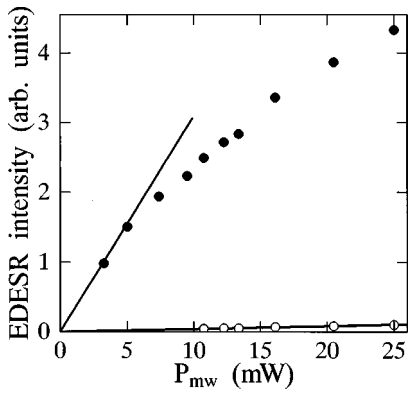

FIG. 4. Integrated EDESR intensities of the central (●) and satellite (○) lines vs microwave power P_{mw} for the *X*-band spectrum of a H_2Pc/C_{60} heterojunction at room temperature. For the straight lines, see the text.

0.50 mT, and the relative integrated intensity of the satellite to the central line is 0.023. The origin of the satellites becomes clear when the magnetic-field dependence of the spacing and the intensity of the satellites is investigated: Figure 3 shows the *K*-band (23 GHz) EDESR spectra with microwave powers of 25 and 0.78 mW. The satellites are seen in the 25-mW spectrum in Fig. 3. A simulation shows that the spacing between the satellite and the central line is 1.25 mT, and the intensity ratio of the satellite to the central line is 0.0040. The ratio of the spacings in the *K*- and *X*-band spectra is 1.25 mT/0.50 mT=2.50 which is very close to the ratio of the magnetic field intensity H_0 for the two spectra, i.e., 826.4 mT/332.4 mT=2.49, indicating that the spacing is proportional to H_0. Such a field dependence is not seen in the usual hyperfine splitting. Furthermore, the ratio of the satellite intensity between the *K*- and *X*-band spectra is 0.0040/0.023=0.17 which is close to $[H_0(K\text{ band})/H_0(X\text{ band})]^{-2}=0.16$, suggesting that the satellite intensity is proportional to H_0^{-2}. The observed magnetic-field dependence of the spacing and the intensity of the satellites is characteristic of the spin-flip satellites.[12,13] The spin-flip satellites are caused by a forbidden transition in which an electron (or hole) spin and its neighboring nuclear spin flip at the same time by the electron spin resonance. It is known that the spacing between a spin-flip satellite and the central line is given by $\mu_n H_0/\mu_e$, where μ_n and μ_e are the magnetic moments of the nucleus and the electron (or hole), respectively, and that the relative intensity of the satellite to the central line is given by $3N\mu_e^2/5H_0^2r^6$, where N is the number of the nuclei surrounding the electron (or hole) and r is the distance between the electron (or hole) and the nuclei. The nuclei responsible for the satellites in the present system are protons since the observed spacing of 0.50 mT in the *X*-band spectrum is identical with the expected value of 0.505 mT for protons within experimental error. Thus it is concluded that the observed satellites in the present system is the spin-flip satellites caused by the interaction of the electron (or hole) spin with their surrounding nuclear spins of protons.

The relative intensity of the satellites to the central line becomes very weak at low microwave power, as is seen in Figs. 2 and 3. The larger relative intensity of the satellites at higher microwave power is due to the power saturation of the central line. The power saturation of the satellites occurs at much higher microwave power because the microwave transition rate for the satellites is much slower than that for the central line. The above-mentioned expression of $3N\mu_e^2/5H_0^2r^6$ is for the limit of low microwave power, where no power saturation occurs for the central line, as well as the satellites. In this limit, the signal intensity has a linear dependence on the microwave power [see Eqs. (2) and (3)]. Figure 4 shows the integrated signal intensities of the central and the satellite lines in the *X*-band EDESR spectrum as a function of the microwave power P_{mw}. The satellite intensity has a linear dependence on P_{mw} in the whole range of the present measurement. On the other hand, the signal intensity of the central line has a linear dependence only below 5 mW. Thus the experimental value for $3N\mu_e^2/5H_0^2r^6$ is obtained from the ratio of the tangents of the two linear lines in Fig. 4, which is 0.015. Since μ_e and H_0 are known, the value of $r/N^{1/6}$ can be estimated, which is 2.6 Å. For the estimation of r, we need to know the number N of the protons surrounding an electron (or hole), which will be discussed in Sec. V B.

The satellite intensity becomes weaker as the temperature is lowered, and the satellites are not detected below 190 K for the *X* band and 250 K for the *K* band when the bias voltage is not applied. By applying a positive or negative bias voltage, the satellites become detectable even at low temperature. These indicate that the mean distance between the electron (or hole) and the protons becomes larger by lowering the temperature, and becomes shorter by applying the bias voltage.

Comparing the calculated and the observed *K*-band EDESR spectra with the microwave power of 25 mW in Fig. 3, a small disagreement is seen between the two at $H_0 \sim 827$ mT. Such a disagreement is not seen for the 0.78 mW spectrum in Fig. 3. The origin of the disagreement becomes clear by observing the spectrum at lower temperature, which is shown in Fig. 5. It is seen in Fig. 5 that a new peak grows up at the higher-field shoulder of the $g=2.0018$ signal as the temperature is lowered. The observed spectra are explained as an overlap of two Lorentzian lines located at $g=2.0018\pm0.0002$ (component *A*) and 2.0010 ± 0.0002 (component

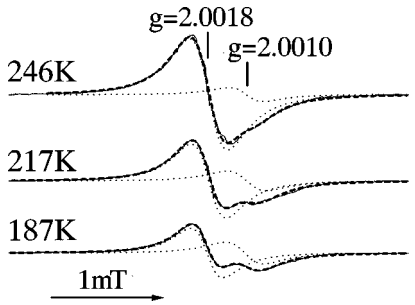

FIG. 5. Temperature dependence of the *K*-band EDESR spectrum of a H_2Pc/C_{60} heterojunction. The microwave power is 25 mW. The broken lines are simulated ones by an overlap of two Lorentzian lines which are shown by the dotted lines.

B), as shown in Fig. 5. The relative intensity of *B* to *A* increases as the temperature is lowered.

Figure 6 shows the microwave power dependence of the *K*-band EDESR spectrum at 204 K. A bias voltage of $V=-0.5$ V was applied in order to obtain a sufficient signal-to-noise ratio. The results of the simulation by the two Lorentzian lines are also shown in Fig. 6. The relative intensity of the component *B* compared to that of component *A* increases as the microwave power increases. The peak-to-peak signal intensity V_{pp} and the linewidth ΔH_{pp} of the two components *A* and *B* are plotted in Fig. 7 as functions of the microwave power P_{mw}. These power saturation results are not explained by a saturation theory for a homogeneously broadened line, but can be explained by assuming an inhomogeneous broadening.[14]

In the case of inhomogeneous broadening,[15,16] an observed EDESR line is assumed to be a result of an overlap of spin packets, i.e., homogeneous lines, the resonant frequency of which has a distribution as a result of, for example, an unresolved hyperfine structure, a distribution in the *g* value, etc. In this case, the observed EDESR line shape is written as

$$V(\omega)=\int_{-\infty}^{\infty} f(\omega-\omega')\, g(\omega'-\omega_0)\, d\omega', \tag{1}$$

where $f(\omega-\omega')$ is the line shape of the spin packet the center of which is ω', and $g(\omega'-\omega_0)$ is the distribution

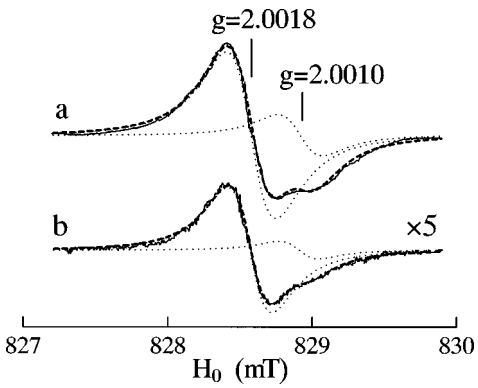

FIG. 6. *K*-band EDESR spectra of a H_2Pc/C_{60} heterojunction at 204 K with microwave powers of 25 mW for *a* and 0.38 mW for *b*. The bias voltage $V=-0.5$ V. The broken lines are simulated ones by an overlap of two Lorentzian lines which are shown by the dotted lines.

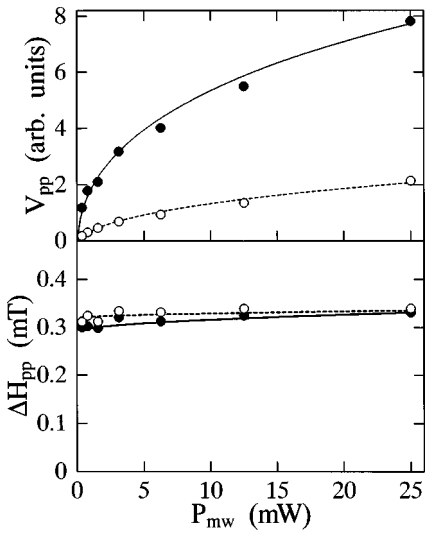

FIG. 7. The microwave power P_{mw} dependence of the peak-to-peak signal intensity V_{pp} and linewidth ΔH_{pp} of the *K*-band EDESR spectrum of a H_2Pc/C_{60} heterojunction at 204 K. ●: For the component *A* at $g=2.0018$. ○: For the component *B* at $g=2.0010$. Bias voltage $V=-0.5$ V. The solid and the broken lines are the theoretical ones in the case of an inhomogeneous broadening, the details of which are described in the text.

function of ω' with ω_0 being the center of the distribution. As will be shown in Sec. IV, and has also been shown by other groups,[4,6] $f(\omega-\omega')$ is generally given by the formula

$$f(\omega-\omega')=C\frac{\beta W_{mw}(\omega-\omega')}{1+\beta W_{mw}(\omega-\omega')}, \tag{2}$$

where $W_{mw}(\omega-\omega')$ is the microwave transition probability between the spin levels, and *C* and β are constants. It is assumed that $W_{mw}(\omega-\omega')$ has a Lorentzian distribution with a half-width of $1/T_2$, i.e.,

$$\beta W_{mw}(\omega-\omega')=\alpha P_{mw}\frac{T_2}{\pi}\frac{1}{1+(\omega-\omega')^2 T_2^2}, \tag{3}$$

where P_{mw} is the microwave power in mW, and α is a constant which is proportional to β and also mechanical constants of the microwave cavity.[17] The distribution function $g(\omega'-\omega_0)$ is assumed to be Lorentzian with a half width of $1/T_2^*$ since the observed EDESR line shape is nearly Lorentzian:

$$g(\omega'-\omega_0)=\frac{T_2^*}{\pi}\frac{1}{1+(\omega'-\omega_0)^2 T_2^{*2}}. \tag{4}$$

The present experiment observes the first derivative line shape $V'(\omega)$ by employing a field modulation, which is, from Eqs. (1)–(4),

$$V'(\omega)=-2CT_2^* \times\int_{-\infty}^{\infty}\frac{q^2\alpha T_2 P_{mw}(x-\xi)}{[q^2(\pi+\alpha T_2 P_{mw})+\pi(x-\xi)^2]^2}\frac{1}{1+\xi^2}\,d\xi, \tag{5}$$

where

$$\xi = T_2^*(\omega' - \omega_0)\,, \tag{6}$$

$$x = T_2^*(\omega - \omega_0)\,, \tag{7}$$

and

$$q = T_2^*/T_2\,. \tag{8}$$

The peak-to-peak signal intensity V_{pp} and linewidth ΔH_{pp} are calculated numerically by using Eq. (5) when the values of the parameters T_2, T_2^*, α, C, and P_{mw} are given. The experimental power saturation behavior in Fig. 7 is well explained by this formalism with the following parameter values: For the lower-field component A, $T_2 = 2.3\,(\pm 0.3) \times 10^{-6}$ s, $T_2^* = 2.3\,(\pm 0.1) \times 10^{-8}$ s, $\alpha_A = 1.1\,(\pm 0.3) \times 10^7$ $\mathrm{s}^{-1}(\mathrm{mW})^{-1}$ and $C_A = 4.9\,(\pm 0.3)$. For the higher-field component B, $T_2 = 2.1\,(\pm 0.3) \times 10^{-6}$ s, $T_2^* = 2.1\,(\pm 0.1) \times 10^{-8}$ s, $\alpha_B = 1.8\,(\pm 0.5) \times 10^6$ $\mathrm{s}^{-1}(\mathrm{mW})^{-1}$, and $C_B = 3.2\,(\pm 0.2)$. Comparing the parameter values for A and B, difference is seen in the α and C values with $\alpha_A/\alpha_B = 6.1 \pm 2.3$ and $C_A/C_B = 1.5 \pm 0.1$. This gives evidence that the two components A and B come from different types of electron-hole pairs, as will be discussed in Sec. V A.

Now the temperature dependence of the EDESR spectrum in Fig. 5 is considered. The relative intensity of component B compared to that of component A, increases as the temperature is lowered. This is attributed mainly to a strong temperature dependence of α, which is, as shown in Eqs. (45)–(47), a function of the generation (k), the dissociation (D), the recombination (R), and the spin-lattice relaxation (W_{sl}) rates of the localized electron-hole pairs and the response rate (W_c) of the detection circuit, with D, W_{sl}, and W_c dependent on temperature. Furthermore, while components A and B are attributed to different types of localized pairs, the relative number of the localized pairs A and B may also be temperature dependent. Thus there are too many parameters that determine the temperature dependence in Fig. 5, so that no quantitative analysis is possible.

In the present EDESR spectrum, spin-flip satellites are observed at room temperature. The satellites belong to the lower-field component A since, as seen in Figs. 2 and 3, the two satellites locate at an even distance from the field corresponding to $g = 2.0018$ which is the center of component A. This is confirmed by observing the X-band spectrum at 169 K with a bias voltage of $V = -1.0$ V which is shown in Fig. 8. In Fig. 8, the overlap of the two components A and B are clearly seen, and at the same time, one of the satellites is seen at 331.07 mT, but the other satellite is hidden in the tail of the component B. The observed satellite at 331.07 mT should belong to the component whose center locates at 331.07 mT+0.505 mT=331.575 mT, i.e., component A, where 0.505 mT is the spacing between the central and satellite lines for the proton-spin-flip in the X-band spectrum. Thus, the spin-flip satellites belong to the lower-field component A.

B. Microwave recovery

Microwave recovery experiment was done for the H_2Pc/C_{60} heterojunction, in which the time dependence of the photocurrent was measured after turning the microwave at the center of the resonance on and off. Figure 9 shows the recovery curves at room temperature. Since the EDESR signal intensity of component B is negligibly weak at room temperature, the recovery curves in Fig. 9 are attributed solely to component A. As seen in Fig. 9, the photocurrent decreases by a factor of 6.2×10^{-4} by turning on the microwave. The recovery curve after turning on or off the microwave is not explained by a monoexponential function, but is explained by an overlap of two or more exponential functions with different recovery rates. Figure 9 shows a result of a fitting assuming a Gaussian distribution for the rate

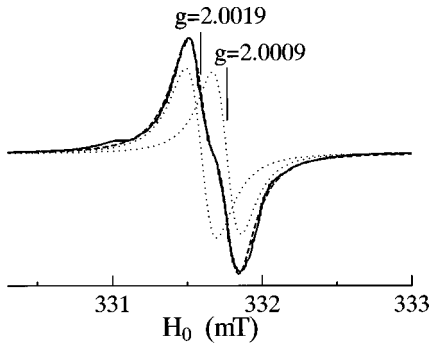

FIG. 8. X-band EDESR spectrum of a H_2Pc/C_{60} heterojunction at 169 K. Bias voltage $V = -1.0$ V. The broken line is a simulated one by an overlap of two Lorentzian lines which are shown by the dotted lines.

$$I(t) = I(\infty) - \{I(\infty) - I(0)\} \frac{\int_0^\infty e^{-Wt} h(W)\,dW}{\int_0^\infty h(W)\,dW}, \tag{9}$$

where

$$h(W) = \frac{1}{\sqrt{2\pi}D} \exp\left[-\frac{(W - W_0)^2}{2D^2} \right]. \tag{10}$$

In Eq. (9), $I(t)$ is the photocurrent at time t, the microwave being turned on or off at $t = 0$. For simplicity, it was assumed

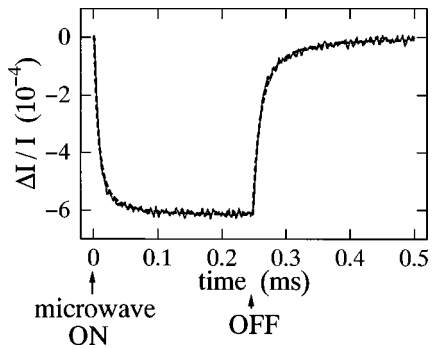

FIG. 9. X-band microwave recovery curves of the photocurrent of a H_2Pc/C_{60} heterojunction at room temperature. The magnetic field H_0 is at the center of the resonance. The broken line is a calculated one with a Gaussian distribution of the recovery rate, the mean recovery rate W_0 being 1.16×10^5 s^{-1} and 6.17×10^4 s^{-1} after turning the microwave on and off, respectively.

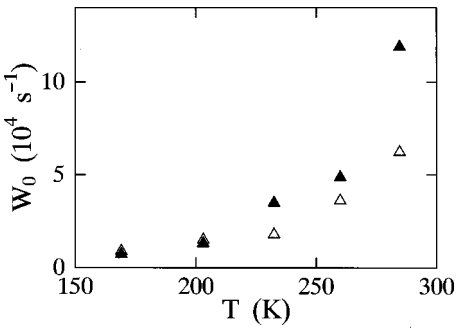

FIG. 10. Temperature dependence of a mean recovery rate W_0 of the photocurrent of a H_2Pc/C_{60} heterojunction after turning the microwave on (▲) and off (△).

in the fitting that $D=W_0$, so that the fitting parameters were W_0, $I(0)$, and $I(\infty)$. Since the experimental recovery curve can also be fitted by other distribution functions $h(W)$, it is not possible to determine uniquely the function form of $h(W)$. Here the value of W_0 obtained by the fitting with Eq. (10) is used in order to represent the recovery rate of the experimental data.

The values of W_0 after turning the microwave on and off are 1.16×10^5 and 6.17×10^4 s^{-1}, respectively. The 1.9 times larger value of W_0 after turning on is attributed to the occurrence of the microwave transition between the spin levels, which enhances the recovery rate of the photocurrent. This gives an evidence that the present microwave recovery experiment observes the spin dynamics of the localized electron-hole pairs. A more detailed explanation of the experimental recovery curves will be given after presenting a theoretical model of the spin-dependent recombination in Sec. IV.

Figure 10 shows the temperature dependence of W_0 after turning the microwave on and off. It is seen that W_0 decreases steeply as the temperature is lowered. As shown in Sec. IV, W_0 is a function of the generation (k), the dissociation (D), the recombination (R), the spin-lattice relaxation (W_{sl}), and the microwave transition (W_{mw}) rates of the electron-hole pairs and the response rate (W_c) of the detection circuit, with D, W_{sl}, and W_c being temperature dependent. If W_c is larger than the other rates, W_0 is roughly approximated by Eq. (48), and the decrease of W_0 at low temperature is attributed to a decrease of D and W_{sl}. In this case, the difference between the W_0 values after turning the microwave on and off would be $\sim W_{mw}$, which is nearly temperature independent. In Fig. 10, however, the W_0 values after turning the microwave on and off become almost identical at $T\lesssim200$ K. This is explained by the temperature dependence of W_c: In the present heterojunction, the resistance of the sample increases steeply as the temperature is lowered. The large resistance of the sample makes the response rate W_c of the detection circuit slower. It is interpreted that W_c becomes of the same order as or even smaller than the other rates at low temperature, and the observed recovery rate W_0 at $T\lesssim200$ K is mainly determined by W_c. It is also noted that component B begins to contribute to the microwave recovery as the temperature is lowered. Thus the temperature dependence of W_0 in Fig. 10 is explained by the temperature dependence of W_c as well as D and W_{sl}, with some disturbance by component B, and W_0 at $T\lesssim200$ K does not reflect the spin dynamics of the electron-hole pairs.

IV. THEORETICAL MODEL

In the present experiment, a decrease of the photocurrent by a factor of 6.2×10^{-4} was observed at room temperature by turning on the microwave at the center of the resonance. The decrease of the photocurrent is explained by an increase of the recombination probability between the photogenerated electrons and holes. The simplest model to explain the increase of the recombination probability was proposed by Lepine.[1] In this model, it is assumed that the populations of the spin states of the electron and the hole obey the Boltzmann statistics and, if an electron and a hole make a pair in the singlet spin configuration, that recombination can take place. By applying a resonant microwave which causes a saturation of the spin-state populations, the Boltzmann distribution is disturbed, so as to increase the probability of the singlet pair generation. As a result, the recombination probability is increased. In this model, however, the decrease of the photocurrent due to the spin resonance is at most by a factor of 10^{-6} at room temperature, so that the observed decrease of 6.2×10^{-4} is not explained.

The decrease of the photocurrent much larger than 10^{-6} is explained by a localized electron-hole pair model originally proposed in Ref. 2. In this model, an electron and a hole form a localized pair for a certain period. Since the localized pairs in the singlet configuration can disappear due to the recombination, the fraction of the singlet pairs becomes substantially less than that expected by the Boltzmann distribution. By the occurrence of the spin resonance, the spin state in the singlet configuration is populated from the triplet state, and the recombination probability is increased. In this model, a decrease of the photocurrent by a factor of up to 10^{-1} can be explained.

Kaplan, Solomon, and Mott assumed a negligibly weak exchange interaction between the electron and hole, because, if the exchange interaction is stronger than the difference of the resonance frequencies of the electron and the hole, the resonance transition occurs only within the triplet sublevels and the population of the singlet state is not affected. However, as will be discussed in Sec. V A, the spectrum observed in the present EDESR experiment is attributed to exchange-coupled electron-hole pairs. A point of the theoretical model proposed here is that, even under the existence of the exchange interaction, the increase of the recombination probability by the spin resonance occurs through the mixing of the singlet and triplet states. Details are presented below.

In the interface region of the heterojunction, there exist photogenerated carriers. Some of them diffuse out of the interface region to contribute to the photocurrent, and some form localized electron-hole pairs. Some of the localized pairs recombine and the others dissociate to populate the mobile carriers again. This situation is illustrated in Fig. 11(a). Then the rate equation for the number n_c of the photogenerated mobile electron or hole becomes

$$\frac{dn_c}{dt}=G-k\,n_c+D\,n-W_c\,n_c\,, \tag{11}$$

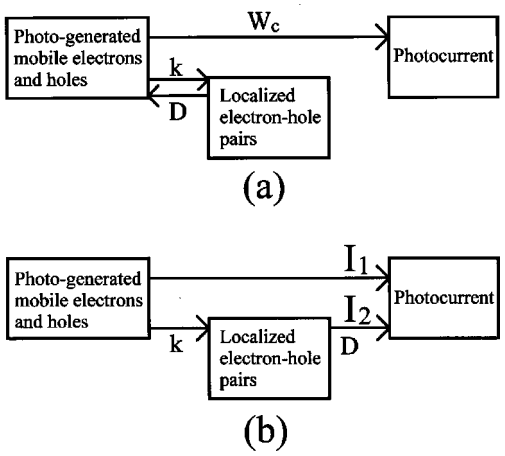

FIG. 11. The relation between the localized electron-hole pairs and the photocurrent. k and D are the rates of the generation and the dissociation of the localized pairs. W_c is the rate at which the carriers escape from the interface region of the heterojunction contributing to the photocurrent. (a) is approximated with (b) when $k \ll W_c$. I_1 and I_2 are the photocurrents by the carriers that have not experienced the localized pairs and have, respectively.

where G is the rate of the charge separation after the photoexcitation, k and D are the rates of the generation and the dissociation of the localized pairs, respectively, the number of which is n, and W_c is the rate that the carriers escape from the interface region contributing to the photocurrent, which is equivalent with the response rate of the detection circuit. The observed photocurrent I is expressed as

$$I = e\, W_c\, n_c\,, \tag{12}$$

where e is the charge of a carrier. If $k \ll W_c$, which is actually fulfilled as shown later, the probability that the dissociated carriers again form the localized pairs becomes negligibly small, so that it is approximated that all the dissociated carriers diffuse out of the interface region and contribute to the photocurrent [Fig. 11(b)]. Defining I_1 and I_2 as the photocurrents generated by the carriers that have not and have formed localized pairs, respectively, the detected photocurrent I becomes

$$I = I_1 + I_2\,. \tag{13}$$

Then what is detected by EDESR is a change ΔI_2 due to the spin resonance. In order to calculate ΔI_2, the rate equations for the populations of the spin states of the localized pairs must be considered, which is done below.

The spin Hamiltonian of the localized electron-hole pair is

$$\mathcal{H} = \mu_0 H_0 (g_e S_{ez} + g_h S_{hz}) + 2J\, \boldsymbol{S_e}\cdot\boldsymbol{S_h}\,, \tag{14}$$

where $\boldsymbol{S_e}$ and $\boldsymbol{S_h}$ are the spin operators of the electron and the hole, respectively, and g_e and g_h are the g values of them. J is the exchange coupling constant, with $J>0$ corresponding to the antiferromagnetic interaction. Using a representation $|S,S_z\rangle$ which diagonalizes the magnitude of $\boldsymbol{S}=\boldsymbol{S_e}+\boldsymbol{S_h}$ and its z component, the eigenfunctions become

$$\psi_1 = |1,1\rangle\,, \tag{15}$$

$$\psi_2 = \sqrt{1-\eta^2}\,|1,0\rangle + \eta\,|0,0\rangle\,, \tag{16}$$

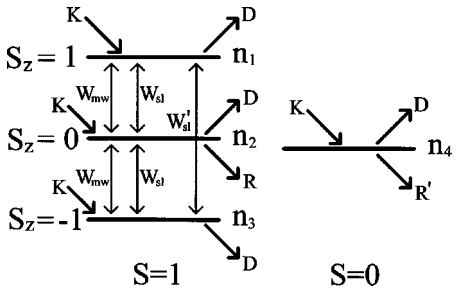

FIG. 12. Energy levels of an exchange-coupled electron-hole pair and the processes governing the populations n_i $(i=1-4)$ of the four spin states. K: Population rate. D: Dissociation rate. R and R': Recombination rates. W_{mw}: Microwave transition rate. W_{sl} and W'_{sl}: Spin lattice relaxation rates.

$$\psi_3 = |1,-1\rangle\,, \tag{17}$$

$$\psi_4 = \sqrt{1-\eta^2}\,|0,0\rangle - \eta\,|1,0\rangle\,, \tag{18}$$

where

$$\eta^2 = \frac{\sqrt{J^2+4(g_e-g_h)^2\mu_B^2H_0^2}-J}{2\sqrt{J^2+4(g_e-g_h)^2\mu_B^2H_0^2}}\,. \tag{19}$$

Assuming that $|J| \gg 2|g_e-g_h|\mu_B H_0$, ψ_1, ψ_2, and ψ_3 correspond to the triplet configuration, and ψ_4 to the singlet. Since ψ_2 includes the $|0,0\rangle$ state by a probability of η^2, the electron-hole recombination can occur in the ψ_2 state as well as in the ψ_4 state, while the recombination rates in the ψ_1 and ψ_3 states are assumed to be zero.

Figure 12 shows the processes governing the populations n_i $(i=1-4)$ of the four states ψ_i. n_i obey the rate equations

$$\frac{dn_1}{dt} = K - Dn_1 - (W_{mw}+W_{sl})(n_1-n_2) - W'_{sl}(n_1-n_3)\,, \tag{20}$$

$$\frac{dn_2}{dt} = K - (D+R)n_2 - (W_{mw}+W_{sl})(2n_2-n_1-n_3)\,, \tag{21}$$

$$\frac{dn_3}{dt} = K - Dn_3 - (W_{mw}+W_{sl})(n_3-n_2) - W'_{sl}(n_3-n_1)\,, \tag{22}$$

$$\frac{dn_4}{dt} = K - Dn_4 - R'n_4\,. \tag{23}$$

In Eqs. (20)–(23), $K=\frac{1}{4}kn_c$ is the population rate of each spin state, which is assumed to be constant since the variation of n_c obtained by turning the microwave on and off is very small under the stationary illumination condition, which is a factor of 6.2×10^{-4} in the present system at room temperature. It is also assumed that the pair is nongeminate, having equal population rates for the four spin levels, which is in contrast to the case of a geminate pair having a finite population rate only for the singlet state. D is the dissociation rate of the localized pairs in the four states $\psi_1-\psi_4$. R and R' are the recombination rates in the ψ_2 and ψ_4 states, respectively. W_{mw} and W_{sl} are the rates of the microwave transition and the spin-lattice relaxation, respectively, between the ψ_1

and ψ_2 or ψ_2 and ψ_3 states. W'_{sl} is the spin-lattice relaxation rate between the ψ_1 and ψ_3 states. The spin-lattice relaxation occurs toward the Boltzmann distribution, which is $n_1=n_2=n_3=n_4$ in the high-temperature approximation. The microwave transition between the ψ_1 and ψ_4 or ψ_3 and ψ_4 states can occur because of the mixing of the $|1,0\rangle$ state in ψ_4, which, however, is neglected because the resonant frequency for this transition is different from that for W_{mw} by $\sim J/2$, and the corresponding EDESR signal has not been detected. Since $R' \gg R$, n_4 is always much smaller than n_1, n_2, and n_3, so that the contribution of n_4 to the photocurrent I_2 is neglected.

Defining N_a and N_b by

$$N_a=n_1+n_3\,, \tag{24}$$

$$N_b=n_2\,, \tag{25}$$

Eqs. (20)–(22) reduce to the two rate equations

$$\frac{dN_a}{dt}=2K-(D+W)N_a+2WN_b\,, \tag{26}$$

$$\frac{dN_b}{dt}=K-(D+R+2W)N_b+WN_a\,, \tag{27}$$

where

$$W=W_{mw}+W_{sl}\,. \tag{28}$$

The solutions of Eqs. (26) and (27) become

$$N_a(t)=A_0+A_1e^{-\lambda_1 t}+A_2e^{-\lambda_2 t}\,, \tag{29}$$

$$N_b(t)=B_0+B_1e^{-\lambda_1 t}+B_2e^{-\lambda_2 t}\,, \tag{30}$$

where

$$\lambda_{1,2}=\tfrac{1}{2}(\,2D+3W+R\pm\sqrt{9W^2+2RW+R^2}\,)\,, \tag{31}$$

so that $\lambda_1>\lambda_2$. In Eqs. (29) and (30),

$$A_0=\frac{2(D+R)+6W}{D(D+R)+(3D+R)W}K\,, \tag{32}$$

$$B_0=\frac{D+3W}{D(D+R)+(3D+R)W}K\,, \tag{33}$$

and A_i and B_i ($i=1$ and 2) are constants having the relations

$$A_{1,2}=\frac{W+R\mp\sqrt{9W^2+2RW+R^2}}{2W}B_{1,2}\,, \tag{34}$$

which are determined by introducing initial conditions.

In the present microwave recovery experiment, the microwave is turned on and off after keeping the microwave off and on, respectively, for long enough periods. Then the initial conditions for $N_a(t)$ and $N_b(t)$ after turning on the microwave at $t=0$ become

$$N_a(0)=A_0+A_1+A_2=A'_0\,, \tag{35}$$

$$N_b(0)=B_0+B_1+B_2=B'_0\,, \tag{36}$$

where A'_0 and B'_0 are the values of A_0 and B_0 in Eqs. (32) and (33) with $W=W_{sl}$, i.e., with the microwave off. Using Eqs. (34)–(36), A_1, A_2, B_1, and B_2 are calculated, the explicit expressions of which are not shown here.

When a condition $\lambda_1 \ll W_c$ as well as $k \ll W_c$ is fulfilled, the photocurrent I_2 is calculated by

$$I_2=e\,D\,(N_a+N_b+n_4)\sim e\,D\,(N_a+N_b)\,, \tag{37}$$

because the dissociated carriers immediately escape the interface region to contribute to the photocurrent in this case. Then, the time dependence of I_2 becomes

$$I_2(t)=I_{20}-C_1e^{-\lambda_1 t}+C_2e^{-\lambda_2 t}\,, \tag{38}$$

where

$$I_{20}=\frac{e\,D\,(3D+2R+9W)}{D(D+R)+(3D+R)W}K \tag{39}$$

and

$$C_{1,2}=\frac{eKDW_{mw}}{Q[Q+(3D+R)W_{mw}]}\frac{3W+R\mp S}{2W}\times\left[\frac{R}{S}(3DW+2WR+DR)\pm DR\right], \tag{40}$$

with

$$S=\sqrt{9W^2+2RW+R^2} \tag{41}$$

and

$$Q=D(D+R)+(3D+R)W_{sl}\,. \tag{42}$$

In Eq. (38), a relation $0<C_1<C_2$ is always satisfied.

Similarly, the photocurrent I'_2 after turning off the microwave at $t=0$ becomes

$$I'_2(t)=I'_{20}+C'_1e^{-\lambda'_1 t}-C'_2e^{-\lambda'_2 t}\,, \tag{43}$$

where the primed quantities are calculated using Eqs. (39)–(41) by replacing W with W_{sl}. Again a relation $0<C'_1<C'_2$ holds.

The EDESR signal intensity V corresponds to the difference of $I'_2(\infty)$ and $I_2(\infty)$, so that

$$V=I'_{20}-I_{20}=\frac{2eKDR^2}{Q(3D+R)}\frac{\dfrac{3D+R}{Q}W_{mw}}{1+\dfrac{3D+R}{Q}W_{mw}}\,. \tag{44}$$

Equation (44) has the same form as Eq. (2).

The above calculations are for the case of $k,\lambda_1 \ll W_c$. Practically, this condition can be relaxed to $k,\lambda_2 \ll W_c$ because a relation $C_1 \ll C_2$ is satisfied in Eq. (38) when $\lambda_1 \gg \lambda_2$, so that the contribution of the $e^{-\lambda_1 t}$ term is neglected in this case. When the serial resistance of the detection circuit in Fig. 1 becomes extremely large, the condition $k,\lambda_2 \ll W_c$ may no longer be fulfilled because the response rate W_c of the circuit becomes small in this case. This situation actually occurs in the low-temperature measurement of the present system where the sample resistance becomes extremely large. In this case, Eq. (11) should be simultaneously

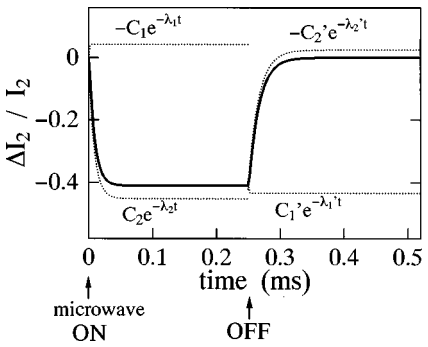

FIG. 13. Theoretical microwave recovery curves calculated by Eqs. (38) and (43). The parameter values are $D=3.2\times10^4$ s^{-1}, $R=1\times10^6$ s^{-1}, $W_{mw}=7.2\times10^4$ s^{-1}, and $W_{sl}=3.2\times10^4$ s^{-1}. The calculated recovery rates are $\lambda_1=1.26\times10^6$ s^{-1} and $\lambda_2=1.17\times10^5$ s^{-1} after turning on the microwave, and $\lambda_1=1.10\times10^6$ s^{-1} and $\lambda_2=6.18\times10^4$ s^{-1} after turning it off.

solved with Eqs. (20)–(23), and the microwave recovery rate becomes to be affected by W_c. Then the EDESR signal intensity V is calculated from the stationary solution for n_c, the result of which is

$$V=e\,W_c\,(n'_{c\,0}-n_{c\,0})=\frac{\frac{1}{2}keGDR^2W_c}{PF}\,\frac{\frac{F}{P}W_{mw}}{1+\frac{F}{P}W_{mw}}, \tag{45}$$

where $n_{c\,0}$ and $n'_{c\,0}$ are the stationary solutions for n_c with the microwave on and off, respectively, and P and F are defined as follows:

$$P=\tfrac{1}{4}k\,[D(D+2R)+(3D+4R)W_{sl}]+W_cQ\,, \tag{46}$$

$$F=\tfrac{1}{4}k(3D+4R)+W_c(3D+R)\,. \tag{47}$$

Again, the EDESR signal intensity has the same form as Eq. (2). As expected, Eq. (45) becomes Eq. (44) in the limit of $k \ll W_c$ since a relation $n_c \sim G/W_c$ is fulfilled in this case.

In the present microwave recovery experiment for component A at room temperature, the observed recovery rate certainly reflects the spin dynamics, since the recovery rates after turning on and off the microwave is different. This indicates that W_c does not affect the microwave recovery rate so that the condition $k,\ \lambda_2 \ll W_c$ is satisfied. Using Eqs. (38) and (43), the theoretical microwave recovery curve is calculated when the values of D, R, W_{mw}, and W_{sl} are given. Figure 13 shows the calculated recovery curves. A recovery curve is made of an overlap of two exponential components $-C_1\,e^{-\lambda_1 t}$ and $C_2\,e^{-\lambda_2 t}$ (or $C_1'\,e^{-\lambda_1' t}$ and $-C_2'\,e^{-\lambda_2' t}$) with $\lambda_1>\lambda_2$ and $C_1<C_2$ (or $\lambda_1'>\lambda_2'$ and $C_1'<C_2'$). The decays of the two components are always in the opposite directions since C_1, C_2, C_1', and C_2' are all positive. In the experimental recovery curves, however, the overlap of the $-C_1\,e^{-\lambda_1 t}$ (or $C_1'\,e^{-\lambda_1' t}$) component is not observed. This indicates that $C_1 \ll C_2$ and $C_1' \ll C_2'$. It is found by inspecting Eq. (40) that these relations are satisfied when a condition $R \gg D, W_{mw}, W_{sl}$ is fulfilled. In this case, the experimental decay rate W_0 corresponds to λ_2 in Eq. (31), which is roughly approximated as

$$W_0 \sim \lambda_2 \sim D+W_{sl}+W_{mw}\,. \tag{48}$$

In the present system at room temperature, W_0 after turning on the microwave is larger than that after turning off. This occurs when $R \gg W_{mw} \gtrsim D, W_{sl}$. The experimental values of $W_0=1.16\times10^5$ and 6.17×10^4 s^{-1} after turning the microwave on and off are explained with $R \gtrsim 1\times10^6$ s^{-1}, $D+W_{sl}=6.2\,(\pm0.8)\times10^4$ s^{-1}, and $W_{mw}=6.4\,(\pm1.0)\times10^4$ s^{-1}.

With the above parameter values, the relative change of the photocurrent by the spin resonance, i.e., $-\Delta I_2/I_2 \equiv (I'_{20}-I_{20})/I'_{20}$ becomes $4.3\,(\pm0.5)\times10^{-1}$, where I_2 is the photocurrent produced by the dissociation of the localized electron-hole pairs for component A. However, the calculated value of 4.3×10^{-1} is for the case when the microwave excites all the localized pairs for component A. The microwave intensity of 25 mW in the present microwave recovery experiment corresponds to the microwave magnetic field H_1 of the order of 0.01 mT,[17] which means that the microwave excites the spins in a width of 0.01 mT at the center of the resonance. Since the linewidth of the present EDESR spectrum is about 0.3 mT, the microwave excites only about 3% of the localized pairs. Thus the theoretical value of 4.3×10^{-1} for $-\Delta I_2/I_2$ should be reduced to 1.3×10^{-2} for comparison with the experiment. The experiment shows that $-\Delta I_2/I=-\Delta I_2/(I_1+I_2)=6.2\times10^{-4}$, where I_1 is the photocurrent by the carriers that do not experience the localized pairs. Comparing the theory and experiment, it is estimated that $I_2/I_1 \sim I_2/I \sim 0.05$. Thus the photocurrent I_2 that is caused by the dissociation of the localized pairs for component A is about 5% of the total photocurrent.

Component B has a negligibly weak EDESR intensity at room temperature. This is mainly because component B has much smaller values of α and β in Eqs. (2) and (3) than component A, so that the number of localized pairs for the component B might be of the same order as that for component A. However, since the microwave recovery experiment for component B is not possible at room temperature, the contribution of component B to the photocurrent is unknown.

The experimental recovery rate has a distribution, as shown in Sec. III B, which indicates that the value of λ_2 has a distribution. This distribution may originate from the distribution of D and W_{mw}. The distribution of D may be caused by a distribution of the distance between the electron and hole, and that of W_{mw} is attributed to the inhomogeneous broadening, with which different spin packets have different W_{mw}.

Dyakonov *et al.* suggested[7] that the intersystem crossing between the ψ_2 and ψ_4 states may give a recombination path for the localized pairs in the ψ_2 state. In the present study, a theoretical model with such an intersystem crossing has also been tried. In this case, the theoretical microwave recovery curve becomes an overlap of three exponential components, and one of the three components shows a decay in the direction opposite to the observed direction with a relatively large amplitude, which is in contradiction with the experiment. Thus, the effect of the intersystem crossing is neglected in the present system.

Dyakonov, Rösler, and Schwoerer suggested recently,[18] in order to explain their experimental results of photoluminescence-detected-magnetic-resonance (PLDMR) for poly-(*p*-phenylenevinylene) films, that a narrow PLDMR line at $g=2$ is caused by a recombination channel in which the interchain charge-transfer excitons, i.e., the geminate polaron pairs produced by the charge transfer between neighboring chains from the primary intrachain singlet excitons, relax to intrachain triplet excitons through an electron back transfer, followed by a triplet-triplet anihilation to singlets. The present EDESR signal is not attributed to such a triplet-triplet anihilation channel because the signal intensity of the present EDESR spectrum shows a linear dependence on the photocurrent or the light intensity in the weak light intensity region, while in the triplet-triplet anihilation mechanism the signal intensity should be proportional to the square of the photocurrent or the light intensity. In the present model, it is assumed that the recombination rate in the pure triplet states ψ_1 and ψ_3 in Eqs. (15) and (17) is zero. This does not deny the possibility that the triplet electron-hole pairs relax to the intramolecular triplet excitons. Similarly, the electron-hole pairs in the ψ_2 and ψ_4 states in Eqs. (16) and (18) may relax into intramolecular singlet excitons, since these two states contain the $|0,0\rangle$ state. Without triplet-triplet anihilation, however, the decay rate of the triplet excitons to the ground singlet state should be much smaller than that of the singlet excitons by several orders of magnitude, and also smaller than the direct decay rate of the singlet electron-hole pairs into the singlet ground state. Since the triplet excitons hardly decay, they may be transformed to triplet electron-hole pairs again. Thus the recombination path of the pure triplet sublevels ψ_1 and ψ_3 is neglected.

Finally, the theoretical analysis for the case of no exchange interaction between the electron and hole is shown in the Appendix. In this case, the theoretical microwave recovery curve becomes almost identical to that calculated by Eqs. (38) and (43) when the parameter values D, R, W_{mw}, and W_{sl} are the same. Thus it is not possible to judge the existence of the exchange interaction by the microwave recovery experiment.

V. DISCUSSION

A. Origin of the two spectral components

The present EDESR study of the H_2Pc/C_{60} heterojunction shows that two spectral components A and B exist with $g=2.0018$ and 2.0010, respectively. One possibility for the origin of the two components is that the EDESR signals of the electron and hole of the localized pair are detected separately. This occurs when the exchange interaction between the electron and hole is weaker than the difference of the resonance frequencies of them. In this case, the theoretical model described in the Appendix should be applied. In the present power saturation analysis in Fig. 7 for the two components A and B at 204 K, $\alpha_A/\alpha_B=6.1\pm2.3$ and $C_A/C_B=1.5\pm0.1$ are obtained, where α and C are defined in Eqs. (2) and (3). The explicit expression of Eq. (2) would be Eq. (A19) in the Appendix. If the two components A and B are the spectra of the electron and the hole of the localized pair, all the parameter values except W_{mw} in Eq. (A19) should be the same for components A and B, so that β_A/β_B and C_A/C_B should be unity, and, since α is proportional to β, α_A/α_B should also be unity. The experimental values of $\alpha_A/\alpha_B=6.1$ and $C_A/C_B=1.5$ are obviously in contradiction with this expectation. This indicates that the two components A and B are not attributed to the electron and hole of the localized pair. The two spectral components should be attributed to different types of localized electron-hole pairs, each of which has its own values of α, β, and C.

The electron and hole in the localized pair for each spectral component are exchange coupled for the following reasons. (1) Each component consists of a nearly Lorentzian single line. If the exchange interaction is weaker than the difference of the resonance frequencies of the electron and hole, the total spin of the pair is not a good quantum number and the spectra of the electron and the hole should be observed separately,[10] which is in contradiction with the experiment. If either the electron or hole has a much larger spin-lattice relaxation rate than the other, its EDESR spectrum may be broadened and difficult to detect. However, the present system does not contain any heavy atoms that make the spin-lattice relaxation rate large through spin-orbit interaction. If the electron and hole have an identical g value and linewidth, it may not be possible to distinguish whether the observed spectrum is an overlap of the two spectra of the electron and hole or the spectrum of the triplet state due to the exchange interaction. In this case, however, any finite exchange interaction may be sufficient to make the total spin of the electron-hole pair a good quantum number. (2) The existence of the exchange interaction is quite natural since the electron and hole of the localized pair should be in close proximity so as to take part in the recombination. Assuming that the difference in the g values of the electron and hole is in the order of 0.001, an exchange interaction in the order of 10^{-3} K is strong enough to make the signals of the electron and hole meet into a single line.[10] (3) In EDESR studies of most other systems,[1,7,9] a separate observation of the electron and hole signals is not reported. (4) The theoretical model presented in Sec. IV for the exchange-coupled electron-hole pair can explain the experimental results of the microwave recovery.

Thus the present EDESR signal is attributed to the microwave transition between the triplet sublevels. The triplet ESR spectrum usually has a fine structure due to the zero-field splitting which spreads over, for example, 100 mT.[19] The present EDESR spectrum, however, does not have such a fine structure, but has a nearly Lorentzian line shape with a linewidth of ~0.3 mT. This indicates that the present system has a negligibly small zero-field splitting. Assuming that the zero-field splitting is determined by the magnetic dipolar interaction between the electron and hole in the pair, the small zero-field splitting is attributed to a large distance between the electron and hole while they are close enough to be exchange coupled. Since the zero-field splitting is smaller than the linewidth, the electron-hole distance is estimated to be larger than 18 Å. A similar exchange-coupled spin pair with negligibly small zero-field splitting was reported in phosphorus-doped silicon.[20,21]

B. Location of the localized pairs

In the present EDESR spectrum, spin-flip satellites are observed for component A. The satellites are caused by the

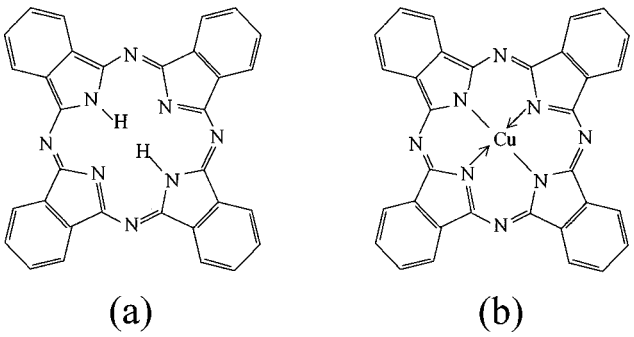

FIG. 14. Structures of (a) H_2Pc and (b) CuPc.

interaction between the electron (or hole) spin and its surrounding nuclear spins of protons. In the present heterojunction, protons exist on the phthalocyanine ring, i.e., two protons at the center and 16 at the edge of the ring [Fig. 14(a)]. The main contribution comes from the edge protons since, as shown in Fig. 15(a), satellites of almost the same intensity are observed even when H_2Pc is replaced by Cu-phthalocyanine (CuPc) which contains no center protons [Fig. 14(b)]. One possibility may be that the hole of the localized pair for component *A* is a H_2Pc^+ radical, and an electron is bound to the hole by the Coulomb interaction. If this is the case, the *g* value of component *A* for $CuPc/C_{60}$ should be different from that for H_2Pc/C_{60}, since the $CuPc^+$ radical should have a different *g* value from that of the H_2Pc^+ radical because of the exchange interaction of the holes with the $S=\frac{1}{2}$ spin on the central metal Cu^{2+}.[22] However, both components *A* and *B* of $CuPc/C_{60}$ have identical *g* values to those of H_2Pc/C_{60}, as shown in Fig. 15(b). Thus the spins of the localized pair of components *A* and *B* do not reside on the Pc rings.

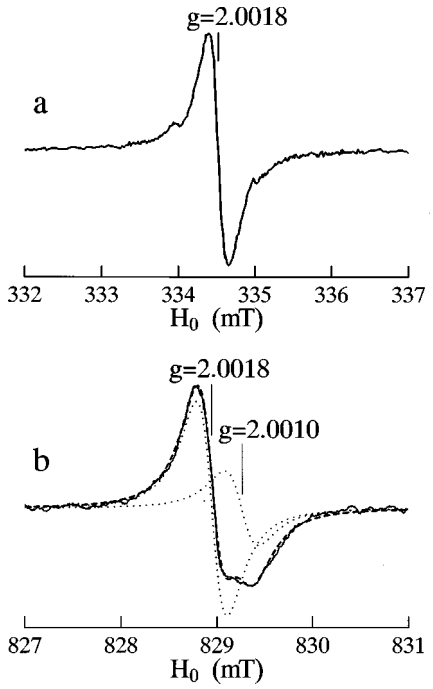

FIG. 15. EDESR spectra of a $CuPc/C_{60}$ heterojunction. (a) *X* band at room temperature. (b) *K* band at 170 K. The broken line for b is a simulated one by an overlap of two Lorentzian lines which are shown by the dotted lines.

In Sec. III A, the value of $r/N^{1/6}$ was estimated to be 2.6 Å from the satellite intensity, where *r* is the distance between the electron (or hole) spin and protons, and *N* is the number of the protons surrounding the electron (or hole) spin. An exact estimation of *N* is impossible, but it is expected that *N* should be in a range between 15 and 30 because the protons responsible for the satellites are the 16 edge protons of the H_2Pc ring. For $N=15$ and 30, *r* becomes 4.08 and 4.58 Å, respectively. Thus, it is concluded that $r=4.33\pm0.25$ Å. This indicates that the localized pair for component *A* is located close to the H_2Pc rings.

The most probable picture of the localized pair is the bound exciton,[23] in which an electron (or hole) is trapped by a recombination center, which is the lattice imperfection or defect having a deep-gap state, and a hole (or electron) is weakly bound to the ionized recombination center by the Coulomb interaction. Since only component *A* has spin-flip satellites, the localized pairs for components *A* and *B* may be located on the recombination centers in the H_2Pc and C_{60} layers, respectively.

VI. CONCLUSIONS

The EDESR spectrum of the H_2Pc/C_{60} heterojunction consists of two components *A* and *B* which have *g* values of 2.0018 ± 0.0002 and 2.0010 ± 0.0002, respectively. The two components are attributed to localized electron-hole pairs trapped at different types of recombination centers. Component *A* has spin-flip satellites due to the interaction between the electron (or hole) spin and the surrounding nuclear spins of protons. From the satellite intensity, the distance between the electron (or hole) and the protons is estimated to be 4.33 ± 0.25 Å, indicating that the localized pairs for component *A* are located close to the H_2Pc rings. By the microwave recovery experiment, the spin dynamics of the localized pair for component *A* was investigated. A theoretical model of the spin-dependent recombination of an exchange-coupled electron-hole pair explains the experimental results of the microwave recovery. By the theoretical analysis, it was found that $R \gtrsim 1\times10^6$ s^{-1} and $D+W_{sl}=6.2(\pm0.8)\times10^4$ s^{-1}. The photocurrent I_2 that is caused by the dissociation of the localized pairs for component *A* is about 5% of the total photocurrent.

APPENDIX: THEORETICAL MODEL IN THE CASE OF NO EXCHANGE INTERACTION

In this appendix, a theoretical model of spin-dependent recombination in the case of negligibly weak exchange interaction between the electron and hole is developed. In this case, S_{ez} and S_{hz} become good quantum numbers, where S_{ez} and S_{hz} are the *z* components of the spins of the electron and hole, respectively. Figure 16 shows the four spin states of the localized electron-hole pair, which are $|S_{ez},S_{hz})=|\frac{1}{2},\frac{1}{2})$, $|\frac{1}{2},-\frac{1}{2})$, $|-\frac{1}{2},\frac{1}{2})$ and $|-\frac{1}{2},-\frac{1}{2})$. The populations n_i $(i=1-4)$ for these spin states obey the following rate equations:

$$\frac{dn_1}{dt}=K-Dn_1-(W^e_{mw}+W^e_{sl})(n_1-n_3)$$
$$-(W^h_{mw}+W^h_{sl})(n_1-n_2)\,, \qquad \text{(A1)}$$

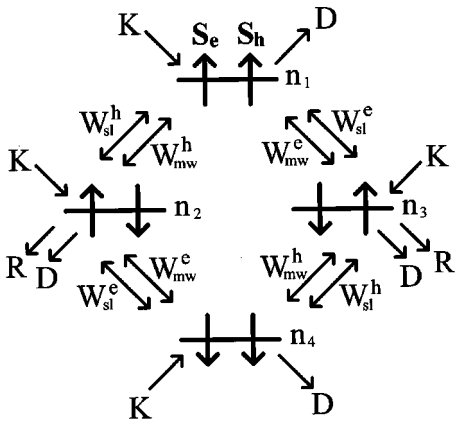

FIG. 16. Energy levels of a localized electron-hole pair in the case of no exchange interaction, and the processes that determine the populations n_i $(i=1-4)$ of the four spin states. K: Population rate. D: Dissociation rate. R: Recombination rate. W_{mw}^e and W_{mw}^h: Microwave transition rates of the electron and the hole. W_{sl}^e and W_{sl}^h: Spin lattice relaxation rates.

$$\frac{dn_2}{dt}=K-Dn_2-Rn_2-(W_{mw}^e+W_{sl}^e)\times(n_2-n_4)-(W_{mw}^h+W_{sl}^h)(n_2-n_1)\,, \tag{A2}$$

$$\frac{dn_3}{dt}=K-Dn_3-Rn_3-(W_{mw}^e+W_{sl}^e)\times(n_3-n_1)-(W_{mw}^h+W_{sl}^h)(n_3-n_4)\,, \tag{A3}$$

$$\frac{dn_4}{dt}=K-Dn_4-(W_{mw}^e+W_{sl}^e)(n_4-n_2)-(W_{mw}^h+W_{sl}^h)(n_4-n_3)\,. \tag{A4}$$

In Eqs. (A1)–(A4), K is the population rate of each spin state. D is the dissociation rate of the localized pair. R is the recombination rate of the electron and the hole which occurs only in the antiparallel spin states $|\frac{1}{2},-\frac{1}{2}\rangle$ and $|-\frac{1}{2},\frac{1}{2}\rangle$, because these states are expressed as linear combinations of the singlet and triplet configurations, and the recombination can occur in the singlet configuration. W_{mw}^e (W_{mw}^h) and W_{sl}^e (W_{sl}^h) are the rates of the microwave transition and the spin-lattice relaxation, respectively, of the electron (hole) spin.

Defining N_p and N_a as the populations of the parallel and the antiparallel states, i.e.,

$$N_p=n_1+n_4\,, \tag{A5}$$

$$N_a=n_2+n_3\,, \tag{A6}$$

Eqs. (A1)–(A4) reduce to the following two rate equations:

$$\frac{dN_p}{dt}=2K-(D+W)N_p+WN_a\,, \tag{A7}$$

$$\frac{dN_a}{dt}=2K-(D+R+W)N_a+WN_p\,, \tag{A8}$$

where

$$W=W_{mw}+W_{sl}\,, \tag{A9}$$

with

$$W_{mw}=W_{mw}^e+W_{mw}^h \tag{A10}$$

and

$$W_{sl}=W_{sl}^e+W_{sl}^h\,. \tag{A11}$$

Solving Eqs. (A7) and (A8) in a similar manner to that in Sec. IV, the time dependence of the photocurrent I_2 after turning on the microwave at $t=0$ becomes

$$I_2(t)=I_{20}-C_1e^{-\lambda_1 t}+C_2e^{-\lambda_2 t}\,, \tag{A12}$$

where

$$\lambda_{1,2}=D+W+\frac{R}{2}\pm\sqrt{W^2+\left(\frac{R}{2}\right)^2}\,, \tag{A13}$$

with

$$I_{20}=\frac{2eKD(4W+2D+R)}{D(D+R)+(2D+R)W}, \tag{A14}$$

and

$$C_{1,2}=\frac{eKDW_{mw}}{Q_a[Q_a+(2D+R)W_{mw}]}\,\frac{W+\frac{R}{2}\mp\sqrt{W^2+\left(\frac{R}{2}\right)^2}}{W}\times\left[\frac{R\left(\frac{DR}{2}+WD+WR\right)}{\sqrt{W^2+\left(\frac{R}{2}\right)^2}}\pm DR\right], \tag{A15}$$

where

$$Q_a=D(D+R)+(2D+R)W_{sl}\,. \tag{A16}$$

In Eq. (A12), relations $\lambda_1>\lambda_2$ and $0<C_1<C_2$ hold.

On the other hand, the time dependence of I_2', after turning off the microwave at $t=0$, becomes

$$I_2'(t)=I_{20}'+C_1'e^{-\lambda_1' t}-C_2'e^{-\lambda_2' t}\,, \tag{A17}$$

where the primed quantities are calculated using Eqs. (A13)–(A15) by replacing W with W_{sl}. Relations $\lambda_1'>\lambda_2'$ and $0<C_1'<C_2'$ again hold. Thus Eqs. (A12) and (A17) are the theoretical expressions for the microwave recovery curves after turning the microwave on and off, respectively.

The EDESR signal intensity V corresponds to the difference of $I_2'(\infty)$ and $I_2(\infty)$, so that

$$V=I_{20}'-I_{20}=\frac{2eKDR^2}{Q_a(2D+R)}\,\frac{\frac{2D+R}{Q_a}W_{mw}}{1+\frac{2D+R}{Q_a}W_{mw}}, \tag{A18}$$

which has the same form as Eq. (2).

When the serial resistance of the detection circuit in Fig. 1 is large, the effect of the response rate of the circuit is not

negligible. In this case, Eq. (11) in Sec. IV must be simultaneously solved with Eqs. (A7) and (A8), and the EDESR intensity V becomes

$$V=\frac{\frac{1}{2}keGDR^2W_c}{P_2F_2}\frac{\frac{F_2}{P_2}W_{mw}}{1+\frac{F_2}{P_2}W_{mw}}, \tag{A19}$$

where

$$P_2=\tfrac{1}{2}k(DR+2RW_{sl})+W_cQ_a\,, \tag{A20}$$

$$F_2=kR+W_c(2D+R)\,. \tag{A21}$$

[1] D. J. Lepine, Phys. Rev. B **6**, 436 (1972).
[2] D. Kaplan, I. Solomon, and N. F. Mott, J. Phys. (France) Lett. **39**, L51 (1978).
[3] A. Maier, A. Grupp, and M. Mehring, Solid State Commun. **99**, 623 (1996).
[4] Z. Xiong and D. J. Miller, Appl. Phys. Lett. **63**, 352 (1993).
[5] I. Hiromitsu, Y. Kaimori, and T. Ito, Solid State Commun. **104**, 511 (1997).
[6] B. Stich, S. Greulich-Weber, and J.-M. Spaeth, J. Appl. Phys. **77**, 1546 (1995).
[7] V. Dyakonov, N. Gauss, G. Rösler, S. Karg, W. Rieß, and M. Schwoerer, Chem. Phys. **189**, 687 (1994).
[8] I. Solomon, Solid State Commun. **20**, 215 (1976).
[9] D. Kaplan and M. Pepper, Solid State Commun. **34**, 803 (1980).
[10] P. W. Anderson, J. Phys. Soc. Jpn. **9**, 316 (1954).
[11] S. Morita, S. B. Lee, A. A. Zakhidov, and K. Yoshino, Mol. Cryst. Liq. Cryst. **256**, 839 (1994).
[12] G. T. Trammell, H. Zeldes, and R. Livingston, Phys. Rev. **110**, 630 (1958).
[13] C. P. Poole and H. A. Farach, J. Magn. Reson. **4**, 312 (1971); **5**, 305 (1971).
[14] A preliminary power saturation analysis was given in Ref. 5. However, a systematic error exists in the derivation of the microwave power in Ref. 5.
[15] A. M. Portis, Phys. Rev. **91**, 1071 (1953).
[16] T. G. Castner, Phys. Rev. **115**, 1506 (1959).
[17] C. P. Poole, *Electron Spin Resonance. A Comprehensive Treatise on Experimental Techniques*, 2nd ed. (Wiley, New York, 1983), Chap. 5H.
[18] V. Dyakonov, G. Rösler, and M. Schwoerer, Phys. Rev. B **56**, 3852 (1997).
[19] N. C. Greenham, J. Shinar, J. Partee, P. A. Lane, O. Amir, and F. Lu, Phys. Rev. B **53**, 13 528 (1996).
[20] G. Feher, Phys. Rev. **114**, 1219 (1959).
[21] D. Jérome and J. M. Winter, Phys. Rev. **134**, A1001 (1964).
[22] M. Y. Ogawa, J. Martinsen, S. M. Palmer, J. L. Stanton, J. Tanaka, R. L. Greene, B. M. Hoffman, and J. A. Ibers, J. Am. Chem. Soc. **109**, 1115 (1987).
[23] O. Madelung, *Introduction to Solid State Theory* (Springer, Berlin, 1978), Chap. 9.